

# A Size-Reduced, Broadband, Bidirectional, Circularly Polarized Antenna for Potential Application in WLAN, WiMAX, 4G, and 5G Frequency Bands

Mason Moore<sup>1</sup>, Zabed Iqbal<sup>2</sup>, and Sungkyun Lim<sup>1, \*</sup>

**Abstract**—A bidirectional, circularly polarized antenna with a miniaturized design and broadband capabilities is proposed for consideration in WLAN 2.4/3.65-GHz, WiMAX 2.3/2.5-GHz, 4G, and 5G frequency bands. The front side of the antenna consists of a hexagonal slot, a hexagonal patch, ten meander tips, and rectangular corner notches to achieve broad impedance and axial ratio bandwidth. The feedline on the backside of the antenna with accompanying shorting pin is offset to further increase the common bandwidth. Also, the four corners of the antenna substrate are removed to decrease the electrical size. The designed antenna is fabricated and measured to validate simulation results. From measured results the antenna has a  $-10$ -dB impedance bandwidth of 89.7% (1.60–4.20 GHz) and a 3-dB axial ratio bandwidth of 70.5% (1.80–3.76 GHz). The peak realized gain in the boresight direction is 3.65 dBi, which occurs at 1.88 GHz.

## 1. INTRODUCTION

Over decades printed antennas have been commonly used in wireless communication systems due to their low-cost structure and low profile. To further increase their appeal in the market for wireless communication systems, extensive research has been done to improve the characteristics of printed antennas for circular polarization (CP) and a broad bandwidth.

CP is used to reduce the effect of multipath interference and polarization mismatch, and a broad bandwidth allows a device to operate in the place of multiple antennas saving space in applied systems. Multiple methods have been designed that can generate CP. CP crossed dipoles as well as bent element parasitic arrays have been researched [1–5]. A slender helical structure with tuning of the circumference and length of the strip allows for CP [6]. Elliptical, square, hexagon, circular, and octagon shaped patches produce CP and have been analyzed [7, 8]. Various techniques have been researched to extend the common bandwidth (CBW) (overlapped bandwidth between  $-10$ -dB impedance bandwidth (IBW) and 3-dB axial ratio bandwidth (ARBW)) of CP antennas. The addition of magneto-electric or stepped edges on dipole elements have been used for broadband CP crossed dipole antennas [9, 10]. Broad CBWs are achieved in patch antennas with parasitic elements, shorting pins, and reactive impedance surfaces [11–13]. Also, antennas with symmetrical slots have been implemented to produce broad CBWs [14–17].

Another key metric that is important to reduce size in applications is the electrical size. The electrical size ( $kr$ ) is a criterion that combines the wave number,  $k$ , and the radius of a sphere,  $r$ , enclosing the antenna to convey an antenna's size according to its wavelength. It is shown from the Chu limit that as  $kr$  gets smaller, so does the radiation efficiency and impedance bandwidth product [18–20]. Thus, a balance between  $kr$  and broad CBW is desired.

---

*Received 18 May 2021, Accepted 6 July 2021, Scheduled 10 July 2021*

\* Corresponding author: Sungkyun Lim (sklim@georgiasouthern.edu).

<sup>1</sup> Department of Electrical and Computer Engineering, Georgia Southern University, Statesboro, GA 30460, USA. <sup>2</sup> Department of Electrical and Computer Engineering, The University of Alabama, Huntsville, AL 25899, USA.

Many of the aforementioned antennas are characterized as unidirectional antennas, but bidirectional antennas are primarily used in two-way communication channels. Bidirectional antennas play important roles in long and narrow communication scenarios like subways, tunnels, bridges, and streets due to obstructions orthogonal to the communication path. Open ended slot ground planes with thin substrates have been used to achieve bidirectional radiation patterns with a broad CBW [21, 22]. Monopole patches with modified geometry have been researched to make CP, bidirectional, and broadband antennas [23–25]. Also, wide-slot antenna designs with alterations to the shape of the slot and/or feedline are used to achieve broadband and CP characteristics while generating bidirectional directivity [26–31].

In this paper, a size-reduced, bidirectional antenna with CP and broad CBW is presented. First, the antenna is designed and simulated in CST Microwave Studio with a series of modifications to improve the CBW while minimizing the electrical size and providing bidirectionality. Then, an analysis of the optimizer is done to show how the Genetic Algorithm (GA) finds the optimum parameters for the cost function. Next, a detailed explanation of the proposed antenna structure is given for important antenna features. The current distribution of the proposed antenna is provided to analyze the generation of CP. Then the antenna is fabricated and measured to validate its CP, broadband, and bidirectional capabilities observed in simulation. The bidirectional nature of the antenna is shown through the measured radiation pattern that propagates opposite sense with equal magnitude in two opposing directions. Finally, a comparison of single feed, broadband, CP, bidirectional antennas and the proposed antenna is presented to analyze the performance with similar works.

## 2. ANTENNA DESIGN

The design procedure of the proposed antenna is shown in Figure 1. Four design iterations, step (a) through (d), are shown with variation between steps. To show the impact of each step, the  $S_{11}$  and axial ratio (in  $+z$  direction) vs. frequency of each step are shown in Figure 2 and Figure 3, respectively. All antennas are designed on a  $54 \times 54 \text{ mm}^2$  sheet of FR4 with a thickness of 1.6 mm, dielectric constant of 4.4, and loss tangent of 0.02.

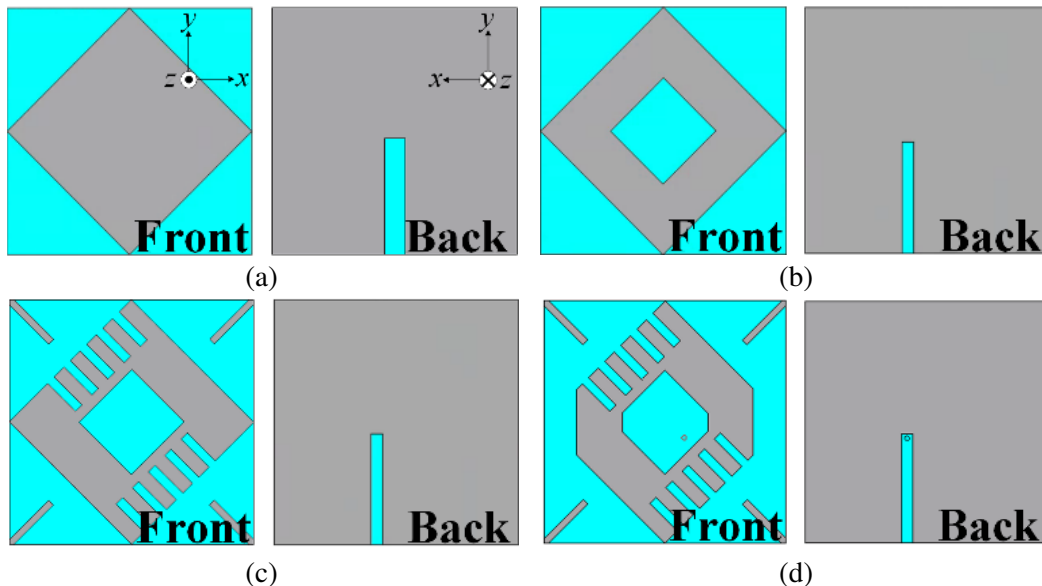


**Figure 1.** Antenna design procedure.

First, as shown in Figure 1(a), a rotated square slot fed by a centered feedline is used for its broadband capabilities [32]. The length of the feedline is based on the  $45^\circ$  rotation angle of the square slot. The side length of the wide slot is chosen to resonate at the lowest frequency possible on the  $54 \times 54 \text{ mm}^2$  sheet of FR4, as larger values will create discontinuities in the middle edges of the ground

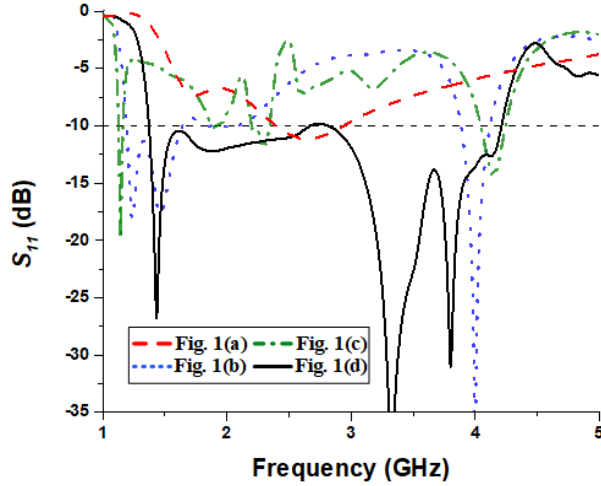


**Figure 2.** Simulated  $S_{11}$  vs frequency of the antenna designs in Figure 1.

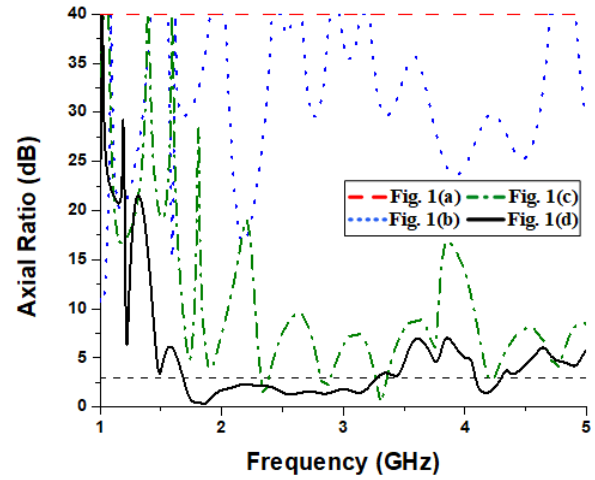


**Figure 3.** Simulated axial ratio vs frequency of the antenna designs in Figure 1.

plane. The minimum  $S_{11}$  occurs at 2.64 GHz providing the antenna with a  $-10$ -dB IBW from 2.40–2.96 GHz or 20.1%. It is noted that at this step the antenna shows no feature for CP as depicted in the axial ratio of Figure 3.

Second, in Figure 1(b), a smaller, offset feedline replaces the previous feedline design, and a parasitic patch is inserted into the center of the rotated slot [33]. The new feedline extends the  $-10$ -dB IBW at the lower end by creating a dual resonance and lowers the axial ratio across the frequency range. The square parasitic patch is rotated at the same angle as the wide slot and adds a new resonant frequency at 4 GHz. The rotated parasitic square patch is used as the feeding structure for the rotated square slot, extending the current path.

Third, the design in Figure 1(c) has diagonal rectangular notches removed from the four corners of the antenna, and meander tips added to two opposing sides of the rotated slot to maintain a symmetrical design. This step reduces the axial ratio closer towards CP, seen in Figure 3, and extends the current path reducing the lowest resonant frequency.

Next, as depicted in Figure 1(d), a shorting pin is inserted between the feedline and center patch [34]. Also, the two opposite, horizontal corners of the rotated square patch and rotated slot are truncated resulting in hexagonal patch and hexagonal slot, respectively. The position of the shorting pin provides broadband matching to  $50\text{-}\Omega$ , extending the  $-10$ -dB IBW drastically from the previous iteration. The placement of the shorting pin plays an integral role in matching by providing a strong current at the connection and lowering the input impedance. The truncations produce CP by generating orthogonal  $E$ -field components at the low and high end of the  $-10$ -dB IBW [7]. The truncations in conjunction with the shorting pin provide a broad ARBW. It is confirmed that the axial ratio in the  $+z$  direction (forward) and  $-z$  direction (backward) are similar, but only the forward direction is given for brevity in Figure 3.

A GA is used in conjunction with CST software to find the optimized antenna design with the broadest CBW and highest realized gain in the forward ( $+z$ ) direction. The cost function for the GA is defined by:

$$\text{Cost} = \sum_{i=1}^{23} \{(S_i + 20) + (AR_i - 1) + (2 - RG_i)\} \text{ [dB]} \quad (1)$$

where  $S_i$  is the  $S_{11}$ ,  $AR_i$  the axial ratio in the forward direction, and  $RG_i$  the realized gain in the forward direction at discrete frequency points. Although the cost function does not include results in the backward ( $-z$ ) direction, preliminary research and tests of printed slot antennas with no ground plane prove that they have bidirectional propagation as they have no structure to direct electromagnetic waves in a single direction [32]. The frequencies for the optimizer are 23 evenly spaced values from 1.5 to 3.8 GHz. The frequency range and number of points are chosen after an initial study to find

the bandwidth of the hexagonal slot and inserted hexagonal patch. Also, the target values for each parameter are chosen to maximize the common bandwidth while maintaining a moderate realized gain across the whole bandwidth. For example, lower values for the targets can create discontinuities in the common bandwidth which drastically reduce the achievable bandwidth. In Figure 4, the value of the lowest cost function at each generation is shown. The fastest change in lowest cost function value occurs in the first 25 generations. After generation 25, there is a drop of only 0.1 dB in the next 40 generations, due to the GA finding parameter values that produce the lowest cost function value in early generations of the optimizer. Future generations begin to converge to a cost function value of 20.8 dB, so further optimizations lead to minor changes in the antenna characteristics.

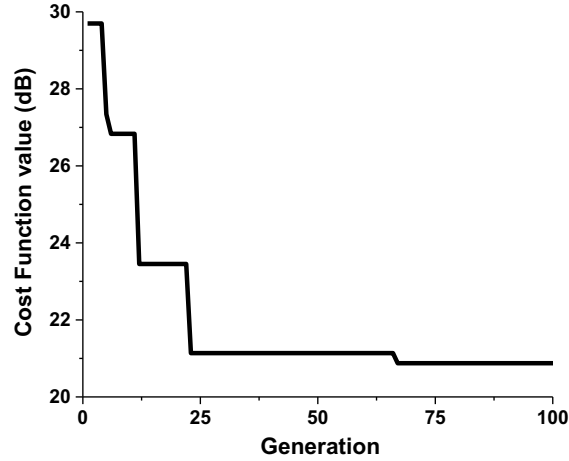


**Figure 4.** Fitness level of the GA optimizer run for the proposed antenna.

## 2.1. Detailed Structure of the Proposed Antenna

The final antenna design is proposed in Figure 5 after further modification and analysis to lower the  $kr$  and improve the CBW. First, the four corners of the antenna substrate are removed to minimize the  $kr$ . The removal depth ( $h$ ) is chosen to minimize  $kr$  as larger values increase the lowest frequency of the CBW and smaller values increase the radius of the sphere enclosing the antenna, both of which increase the  $kr$ . The front side of the antenna, Figure 5(a), consists of the horizontal corner truncated wide

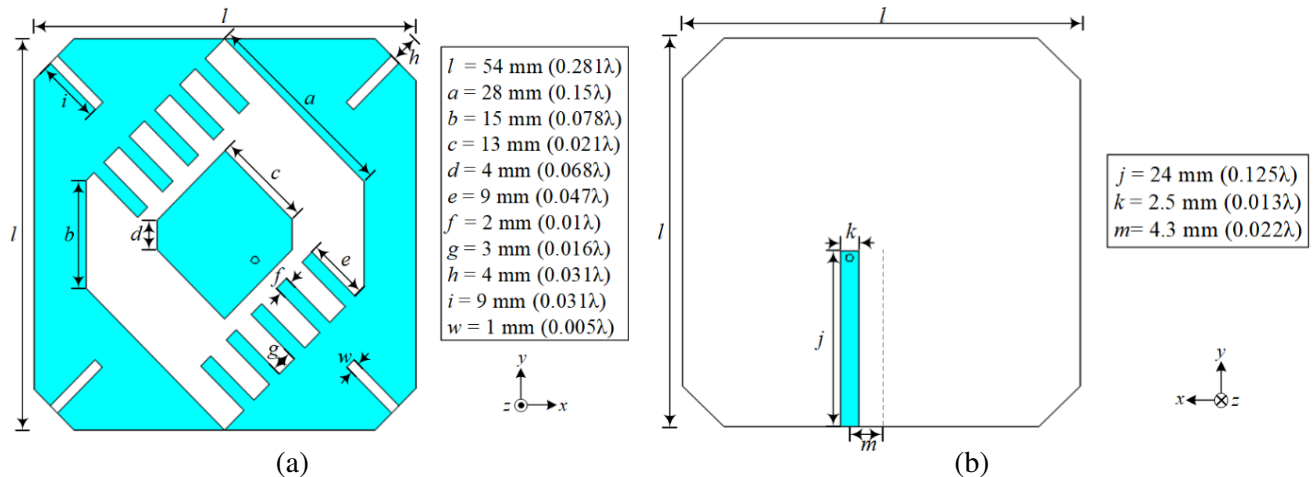


**Figure 5.** The proposed antenna design and dimensions. (a) Frontside and (b) backside.

slot with meander tips, a hexagonal shaped center patch, and diagonal notches on the four removed vertices of the antenna. Long side length ( $a$ ) and short side length ( $b$ ) of the wide slot and the patch's long ( $c$ ) and short ( $d$ ) side lengths are selected to generate the widest CBW as different values create discontinuities in the ARBW. Similarly, the length ( $i$ ) and width ( $w$ ) of the rectangular, diagonal notches on the four corners of the antenna are picked to prevent peaks in the ARBW that jump above 3-dB. The dimensions ( $e$ ,  $f$ , and  $g$ ) of the ten meander tips increase the electrical length and subsequently lower the  $kr$  while maintaining a broad IBW. The number of meander tips are varied to find the proper value that provides the largest CBW. While less than ten meander tips are used, the axial ratio briefly rises above 3-dB reducing the 3-dB ARBW. Also, increasing the number of meander tips beyond ten produces nearly the same  $-10$ -dB IBW. However, the lower bound of the axial ratio is shifted upwards increasing the  $kr$ .

On the backside of the antenna, as depicted in Figure 5(b), the offset feedline is printed with a shorting pin connecting it to the frontside. Feedline length ( $j$ ), width ( $k$ ), and offset ( $m$ ) in conjunction with the shorting pin are chosen for matching. Although the feedline width should be set at 3 mm for proper matching with  $50\text{-}\Omega$  characteristic impedance [35], the shorting pin provides matching to  $50\text{-}\Omega$  between the lowest and highest frequency bands to create one large  $-10$ -dB IBW. These simulated dimensions give the proposed antenna a  $kr$  of 1.31, and the overall volume of the antenna is  $0.33\lambda \times 0.33\lambda \times 0.008\lambda$  ( $54 \times 54 \times 1.6 \text{ mm}^3$ ) where  $\lambda$  is calculated at 1.83 GHz, the lowest simulated frequency of the CBW, which will be discussed in Section 3.

The surface currents at the lowest (1.83 GHz) and highest frequency (3.79 GHz) of the simulated CBW are presented in Figure 6 to analyze the CP operation of the designed antenna. At both frequency bounds the surface current is strong along the feedline, so it is hidden to show the surface current on the hexagonal patch and hexagonal slot clearly, from the frontside. The strong currents are circled with accompanying arrows to show the direction of the current, while transparent, red, small circles are shown at the nulls at  $70^\circ$ . The nulls lie where the currents come together or disperse to cancel each other out. The phase starts at  $70^\circ$  and is increased by  $90^\circ$  intervals. At the lowest frequency, Figure 6(a), from  $160^\circ$  to  $250^\circ$ , the location of the strong current moves from the left and right to the bottom and top of the antenna. The same movement of strong current is observed from  $250^\circ$  to  $340^\circ$  from top and bottom to left and right, as well as from  $340^\circ$  to  $70^\circ$  from left and right to bottom and top. Finally, the strong current moves from top and bottom to left and right from  $70^\circ$  to  $160^\circ$ . Following the direction of the strong current this is a counterclockwise (CCW) rotation, which states the antenna propagates

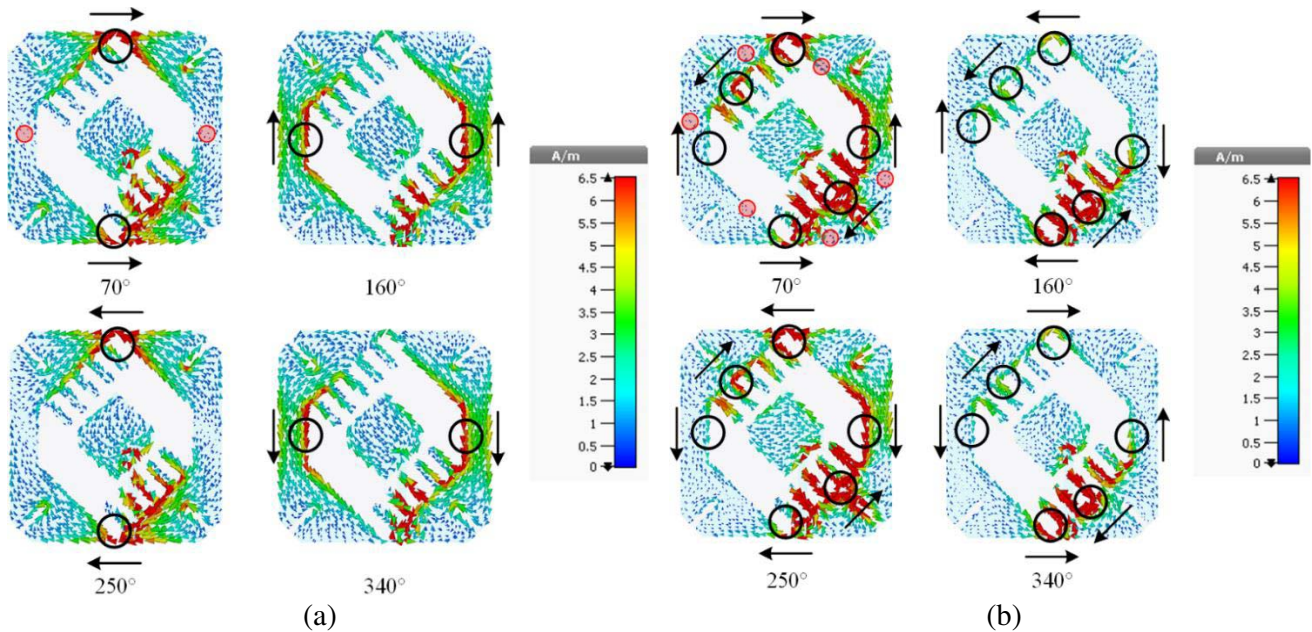


**Figure 6.** The surface current distributions at (a) 1.83 GHz and (b) 3.79 GHz.

RHCP in the  $+z$  direction. It is shown that at the highest frequency, Figure 6(b), there is an increase in number of strong currents and nulls, which coincides with the harmonics of the antenna.

An asymmetrical current distribution is observed at the highest frequency. At  $70^\circ$  and  $250^\circ$ , the magnitudes of strong currents on the left and right sides of the antenna are not equal. The same imbalance of strong current magnitude can be seen at the top and bottom of the antenna, for  $160^\circ$  and  $340^\circ$ . This inequality of magnitude causes a slightly tilted realized gain pattern at the high end of the CBW, which will be discussed in Section 3.

### 3. RESULTS AND DISCUSSION

The proposed antenna is then fabricated, shown in Figure 7, to compare the simulation with measured results. The prototype is measured using an Agilent E5063 network analyzer in an anechoic chamber. The simulated and measured  $S_{11}$  and axial ratio (in the  $+z$  direction) of the proposed antenna are shown in Figure 8(a) and Figure 8(b), respectively. From simulation, a CBW from 1.83–3.79 GHz or 69.8% ( $-10$ -dB IBW of 87.6% [1.59–4.07 GHz] and 3-dB ARBW of 69.8% [1.83–3.79 GHz]) is achieved. Since the forward and backward axial ratio are similar with each other, the axial ratio is only discussed in the forward direction for brevity. The simulated 3-dB axial ratio beamwidths in the front propagation direction for the  $XZ$  and  $YZ$  planes (back propagation direction for the  $XZ$  and  $YZ$  planes) at 2.29 GHz are  $56.3^\circ$  and  $72.5^\circ$  ( $65.2^\circ$  and  $94.1^\circ$ , at 2.78 GHz are  $43.5^\circ$  and  $30.7^\circ$  ( $35.9^\circ$  and  $33.9^\circ$ , and at 3.27 GHz

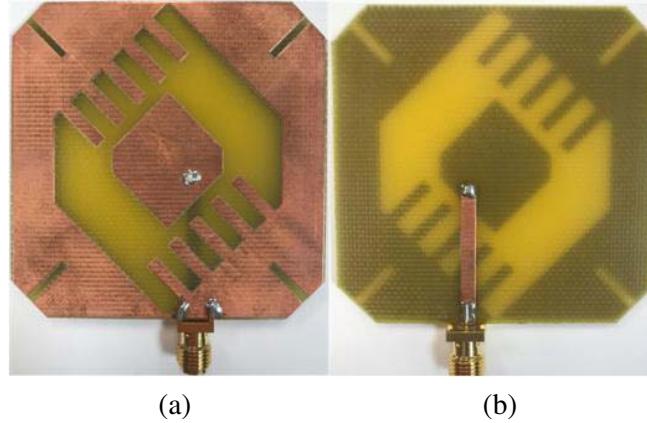


**Figure 7.** The prototype of the proposed antenna. (a) Frontside and (b) backside.

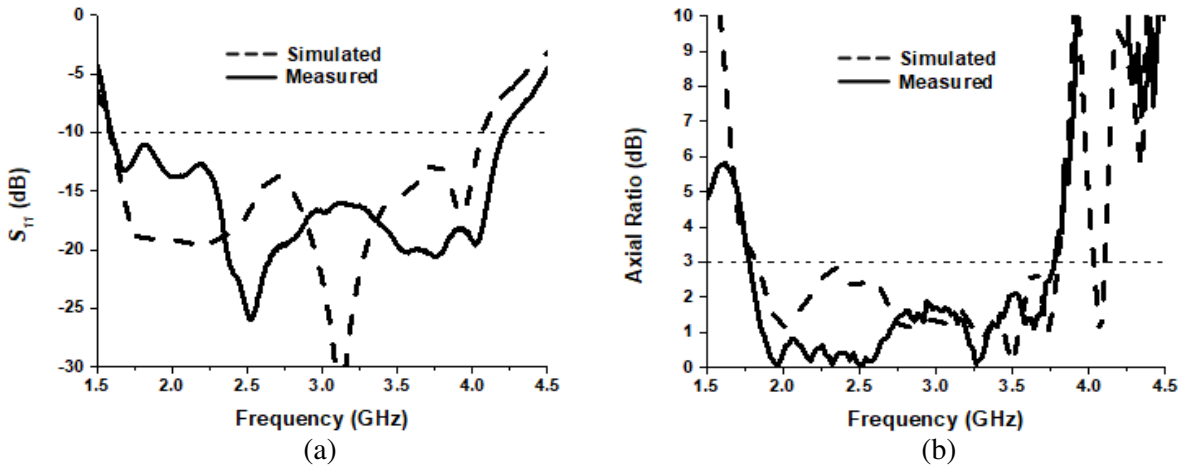


**Figure 8.** The simulated and measured (a)  $S_{11}$  and (b) axial ratio.

are  $32.3^\circ$  and  $24^\circ$  ( $29.3^\circ$  and  $22^\circ$ ). Measurements show a CBW from 1.80–3.76 GHz or 70.5% ( $-10$ -dB IBW of 89.7% [1.60–4.20 GHz] and 3-dB ARBW of 70.5% [1.80–3.76 GHz]). Both measured  $S_{11}$  and axial ratio match well with the simulated results with minimal discrepancies. A minor frequency shift can be seen in the measured  $S_{11}$  compared to the simulated results, which is likely attributed to fabrication errors including addition of the SMA connector.

Figure 9 shows the simulated and measured forward realized gains vs. frequency of the antenna. The backward realized gain is not presented as it is nearly identical to the forward realized gain in simulation, and the bidirectional capability is discussed with the realized gain pattern. The peak forward realized gain in simulation and measurement are similar at 3.48 and 3.6 dBi, respectively.

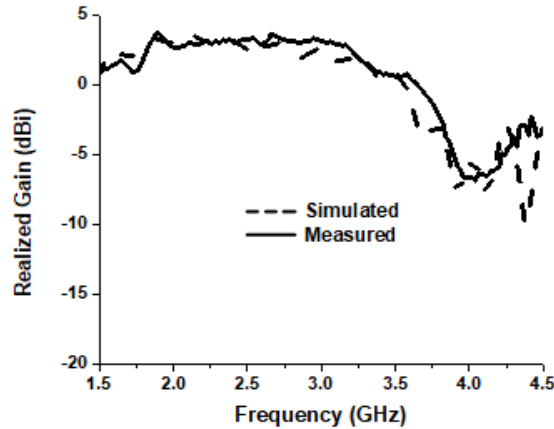


**Figure 9.** The simulated and measured realized gain (in  $+z$  direction) vs. frequency of the proposed antenna.

Next, simulated and measured realized gain patterns for the 25<sup>th</sup> (2.29 GHz), 50<sup>th</sup> (2.78 GHz), and 75<sup>th</sup> (3.27 GHz) percentile of the measured CBW are presented in Figure 10. Measured results agree well with the simulated ones at all three frequencies in both  $XZ$  and  $YZ$  planes. The antenna propagates nearly equal magnitude in the  $+z$  direction and the  $-z$  direction which proves the bidirectional capabilities of the proposed antenna. At the 75<sup>th</sup> percentile, the pattern becomes slightly tilted which is attributed to the less symmetrical surface current at the high end of the frequency band. The realized gain pattern at the 75<sup>th</sup> percentile is still bidirectional, with a 1.8 dBi magnitude at  $0^\circ$  and a 1.5 dBi magnitude at  $180^\circ$  which is only a 1 dBi difference when compared to the realized gain magnitude at the 25<sup>th</sup> percentile  $0^\circ$ . A tilted radiation pattern at higher frequencies is a common issue amongst broadband CP antennas [23, 27, 29].

In Table 1, an extensive comparison of this proposed antenna and other bidirectional, broadband, CP antennas is presented with important characteristics including the lowest frequency in the CBW, overall volume, electrical size ( $kr$ ),  $-10$ -dB IBW, 3-dB ARBW, CBW, and a Figure of Merit. This comparison is limited to single-feed antennas for their ease of manufacturing and low cost. The Figure of Merit is a single value that is defined to compare antennas with multiple performance characteristics more accurately. A higher Figure of Merit corresponds to an antenna with a better combination of CBW and  $kr$ . Subsequently, the Figure of Merit is calculated by the following equation.

$$\text{Figure of Merit} = \frac{\text{CBW}}{\text{Electrical size } (kr)} \quad (2)$$

Table 1 shows that the proposed antenna has the greatest Figure of Merit with 0.53. Note that the antenna with the closest Figure of Merit to the proposed antenna is [23]. The Quasi Monopole design presented in [23] has a slightly smaller electrical size than the proposed antenna. However, the design has a narrower CBW, than this work, by 17.5% leading to a smaller Figure of Merit. From the comparison table, it is shown that the proposed antenna has the widest CBW and a comparable electrical size to similar antennas presented in references.

**Table 1.** Comparison of bidirectional, broadband, CP antennas.

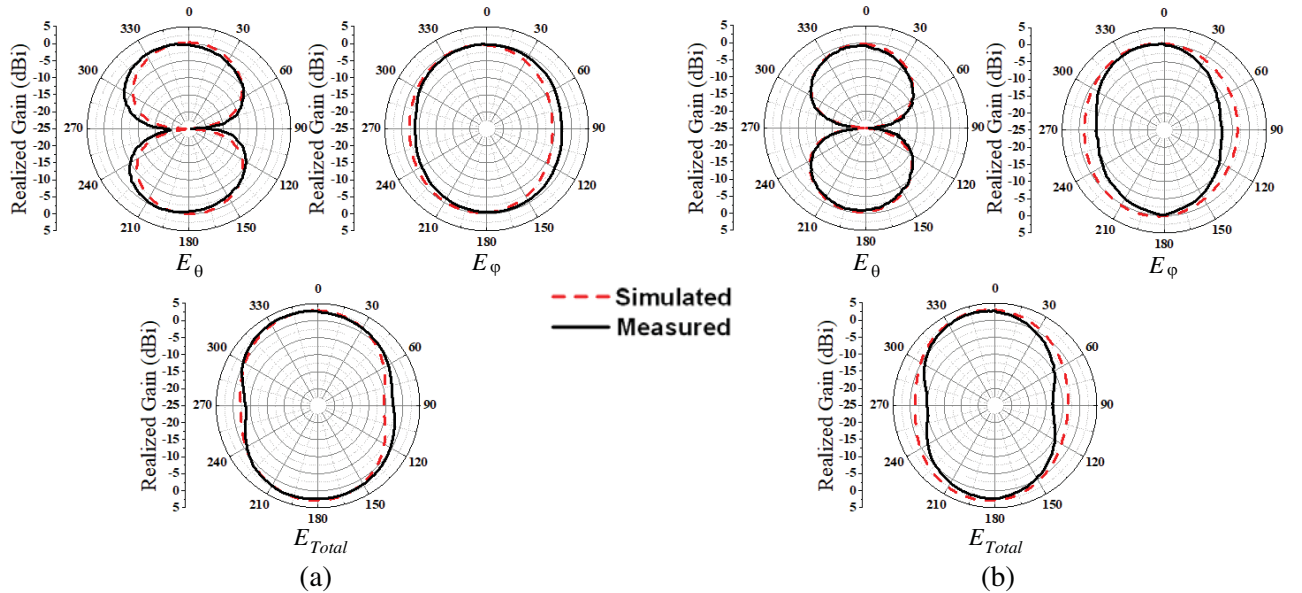
Property	Frequency, $f_L$ (GHz)	Overall Volume ( $\lambda_L^3$ )	Electrical Size ( $kr$ )	-10-dB IBW (GHz)	3-dB ARBW (GHz)	CBW (GHz)	Figure of Merit
[21]	4.09	$0.34\lambda_L \times 0.36\lambda_L \times 0.05\lambda_L$	1.61	3.88–8.02 (69.6%)	4.09–6.55 (46.2%)	4.09–6.55 (46.2%)	0.29
[22]	3.05	$0.51\lambda_L \times 0.51\lambda_L \times 0.008\lambda_L$	2.26	2.0–7.25 (113%)	3.05–4.20 (31.7%)	3.05–4.20 (31.7%)	0.14
[23]	1.71	$0.29\lambda_L \times 0.29\lambda_L \times 0.006\lambda_L$	1.27	1.71–3.42* (66%)	1.70–2.92 (52.8%)	1.71–2.92 (52.3%)	0.41
[24]	2.25	$0.47\lambda_L \times 0.56\lambda_L \times 0.012\lambda_L$	2.31	1.70–3.80 (76.4%)	2.25–2.90 (25.2%)	2.25–2.90 (25.2%)	0.11
[25]	4.78	$0.26\lambda_L \times 0.35\lambda_L \times 0.02\lambda_L$	1.37	4.30–7.60 (55.4%)	4.78–7.10 (39%)	4.78–7.10 (39%)	0.28
[26]	1.70	$0.34\lambda_L \times 0.34\lambda_L \times 0.005\lambda_L$	1.51	1.55–3.35 (73.5%)	1.70–3.11 (58.6%)	1.70–3.11 (58.6%)	0.39
[27]	3.75	$0.34\lambda_L \times 0.36\lambda_L \times 0.01\lambda_L$	1.55	3.75–7.00** (60.5%)	3.60–6.00*** (50%)	3.75–6.00 (46.2%)	0.30
[28]	4.85	$0.40\lambda_L \times 0.40\lambda_L \times 0.026\lambda_L$	1.80	3.20–9.10 (95.9%)	4.85–7.10 (37.7%)	4.85–7.10 (37.7%)	0.21
[29]	4.40	$0.41\lambda_L \times 0.41\lambda_L \times 0.015\lambda_L$	1.83	3.00**–7.25 (82.9%)	4.40–6.55 (39.3%)	4.40–6.55 (39.3%)	0.21
[30]	5.15	$0.34\lambda_L \times 0.34\lambda_L \times 0.01\lambda_L$	1.53	4.75–6.25 (38.1%)	5.15–5.85 (12.7%)	5.15–5.85 (12.7%)	0.08
[31]	9.60	$0.63\lambda_L \times 0.51\lambda_L \times 0.02\lambda_L$	2.54	9.20–12.8 (32.7%)	9.60–12.8 (28.6%)	9.6–12.8 (28.6%)	0.11
This Work	1.83	$0.33\lambda_L \times 0.33\lambda_L \times 0.01\lambda_L$	1.31	1.59–4.07 (87.6%)	1.83–3.79 (69.8%)	1.83–3.79 (69.8%)	0.53

Note: All values are from simulation results since some antennas do not have measurement results. Electrical size is calculated from the lowest frequency ( $f_L$ ) in the CBW, and  $\lambda_L$  is the wavelength calculated from  $f_L$ .

\*The author used VSWR < 2.

\*\*Value given extends past the limits of the graph, so the last value is used.

\*\*\*The axial ratio goes above 3 dB between 4.5 GHz and 4.6 GHz.



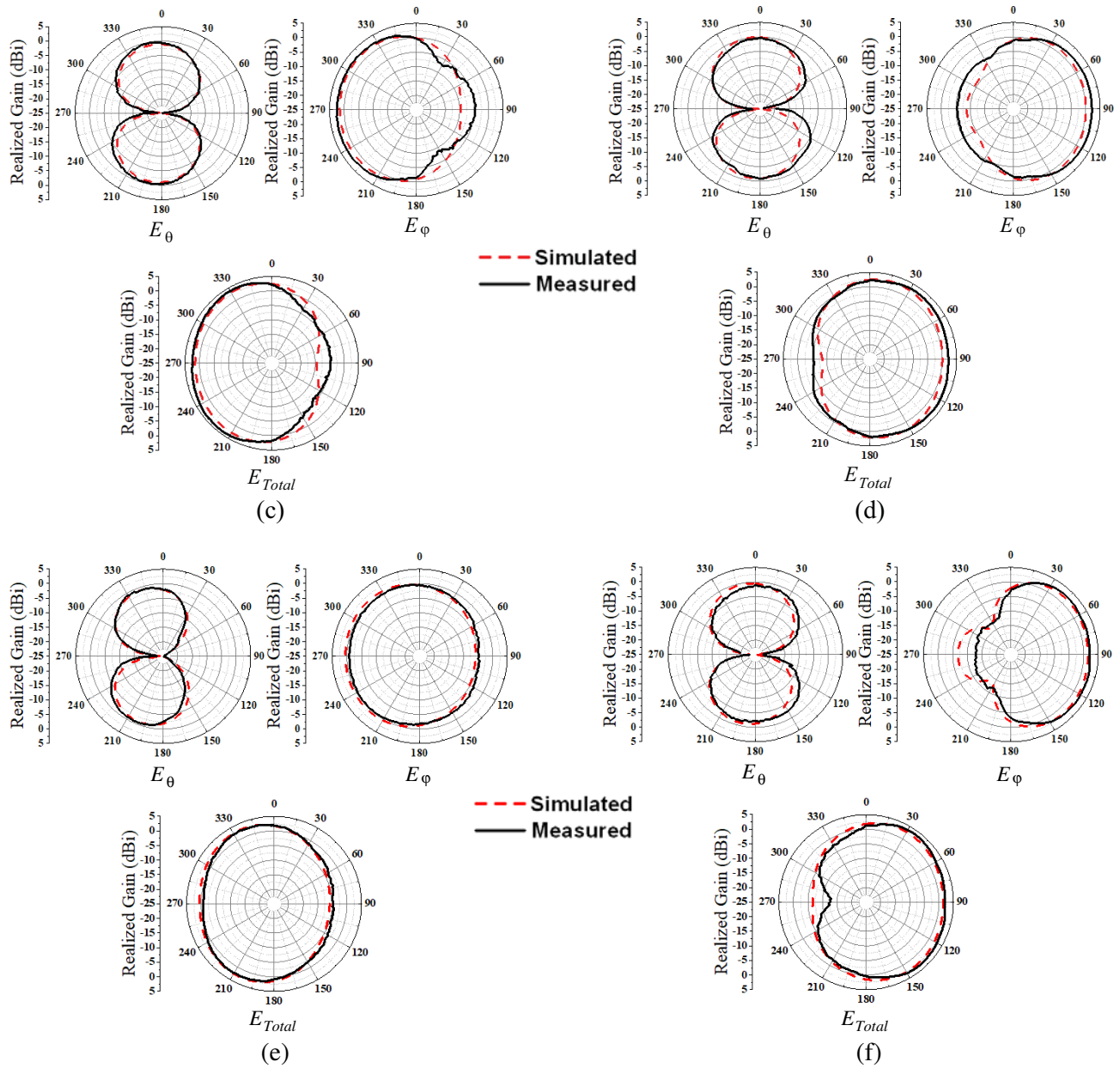


**Figure 10.** Realized gain patterns at 2.29 GHz in (a)  $XZ$  plane, (b)  $YZ$  plane, at 2.78 GHz in (c)  $XZ$  plane, (d)  $YZ$  plane, and at 3.27 GHz in (e)  $XZ$  plane, (f)  $YZ$  plane.

#### 4. CONCLUSION

A size-reduced, broadband, CP antenna printed on an FR4 substrate is proposed to achieve bidirectionality. A prototype of the antenna is constructed and measured to verify results obtained from simulation. The electrical size of the antenna is a  $kr$  of 1.31. The measured results show a CBW of 70.5% from 1.80 to 3.76 GHz, with minimal differences from the simulated antenna. The proposed antenna has a peak forward realized gain of 3.65 dBi at 1.88 GHz. The backward realized gain is similar to the forward realized gain. Due to its reduced size, broad CBW, CP, and bidirectional radiation pattern, this antenna is suitable for multiple frequency bands in several WLAN, WiMAX, 4G, and 5G bands for long and narrow application scenarios.

## REFERENCES

1. Bolster, M. F., "A new type of circular polarizer using crossed dipoles," *IRE Trans. Microw. Theory Tech.*, Vol. 9, No. 9, 385–388, Sep. 1961.
2. Tran, H. H., S. X. Ta, and I. Park, "A compact circularly polarized crossed-dipole antenna for an RFID tag," *IEEE Antennas Wireless Propag. Lett.*, Vol. 14, 674–677, Dec. 2014.
3. Ta, S. X., I. Park, and R. W. Ziolkowski, "Crossed dipole antennas: A review," *IEEE Antennas Propag. Magazine*, Vol. 57, No. 5, 107–122, Oct. 2015.
4. Lim, S., J. Chen, and C. Cato, "Design of a thin, electrically small, two-element parasitic array with circular polarization," *IEEE Antennas Wireless Propag. Lett.*, Vol. 17, No. 6, 1006–1009, Jun. 2018.
5. Yu, J. J. and S. Lim, "Design of an electrically small, circularly polarized, parasitic array antenna for an active 433.92-MHz RFID handheld reader," *IEEE Trans. Antennas Propag.*, Vol. 60, No. 5, 2549–2554, May 2012.
6. Zhang, Y. and T. Fukusako, "Design of circularly polarized low-profile and slender antenna with a helical element," *IEEE Antennas Wireless Propag. Lett.*, Vol. 11, 523–526, May 2012.
7. Gao, S. S., Q. Luo, and F. Zhu, *Circularly Polarized Antennas*, Wiley, Hoboken, NJ, USA, 2014.
8. Shi, Y. and J. Liu, "A circularly polarized octagon-star-shaped microstrip patch antenna with conical radiation pattern," *IEEE Trans. Antennas Propag.*, Vol. 66, No. 4, 2073–2078, Apr. 2018.
9. Ta, S. X. and I. Park, "Crossed dipole loaded with magneto-electric dipole for wideband and wide-beam circularly polarized radiation," *IEEE Antennas Wireless Propag. Lett.*, Vol. 14, 358–361, Oct. 2014.
10. Yang, W., Y. Pan, S. Zheng, and P. Hu, "A low-profile wideband circularly polarized crossed-dipole antenna," *IEEE Antennas Wireless Propag. Lett.*, Vol. 16, 2126–2129, May 2017.
11. Guo, Y.-X. and D. C. H. Tan, "Wideband single-feed circularly polarized patch antenna with conical radiation pattern," *IEEE Antennas Wireless Propag. Lett.*, Vol. 8, 924–926, Jul. 2009.
12. Sun, C., Z. Wu, and B. Bai, "A novel compact wideband patch antenna for GNSS application," *IEEE Trans. Antennas Propag.*, Vol. 65, No. 12, 7334–7339, Dec. 2017.
13. Chatterjee, J., A. Mohan, and V. Dixit, "Broadband circularly polarized H-shaped patch antenna using reactive impedance surface," *IEEE Antennas Wireless Propag. Lett.*, Vol. 17, No. 4, 625–628, Apr. 2018.
14. Lam, K. Y., K.-M. Luk, K. F. Lee, H. Wong, and K. B. Ng, "Small circularly polarized U-slot wideband patch antenna," *IEEE Antennas Wireless Propag. Lett.*, Vol. 10, 87–90, Feb. 2011.
15. Zhang, H., Y. Guo, and G. Wang, "A wideband circularly polarized crossed-slot antenna with stable phase center," *IEEE Antennas Wireless Propag. Lett.*, Vol. 18, No. 5, 941–945, May 2019.
16. Chen, J.-M. and J.-S. Row, "Wideband circularly polarized slotted-patch antenna with a reflector," *IEEE Antennas Wireless Propag. Lett.*, Vol. 14, 575–578, Nov. 2014.
17. Wei, J., X. Jiang, and L. Peng, "Ultrawideband and high-gain circularly polarized antenna with double-y-shape slot," *IEEE Antennas Wireless Propag. Lett.*, Vol. 16, 1508–1511, Jan. 2017.
18. Chu, L. J., "Physical limitations of omni-directional antennas," *J. Appl. Phys.*, Vol. 19, No. 12, 1163–1175, Dec. 1948.
19. Sievenpiper, D. F., et al., "Experimental validation of performance limits and design guidelines for small antennas," *IEEE Trans. Antennas Propag.*, Vol. 60, No. 1, 8–19, Jan. 2012.
20. Smith, L., J. Howell, and S. Lim, "A size-reduced, 15-element, planar Yagi antenna," *IEEE Trans. Antennas Propag.*, Vol. 69, No. 4, 2410–2415, 2021.
21. Lu, L., Y.-C. Jiao, H. Zhang, R. Wang, and T. Li, "Wideband circularly polarized antenna with stair-shaped dielectric resonator and open-ended slot ground," *IEEE Antennas Wireless Propag. Lett.*, Vol. 15, 1755–1758, Feb. 2016.
22. Jan, J.-Y., C.-Y. Pan, K.-Y. Chiu, and H.-M. Chen, "Broadband CPW-fed circularly-polarized slot antenna with an open slot," *IEEE Trans. Antennas Propag.*, Vol. 61, No. 3, 1418–1422, Mar. 2013.

23. Bagheroghli, H., "A novel circularly polarized microstrip antenna with two connected quasi monopoles for wideband applications," *IEEE Antennas Wireless Propag. Lett.*, Vol. 12, 1343–1346, Oct. 2013.
24. Saini, R. K., S. Dwari, and M. K. Mandal, "CPW-fed dual-band dual-sense circularly polarized monopole antenna," *IEEE Antennas Wireless Propag. Lett.*, Vol. 16, 2497–2500, Jul. 2017.
25. Gyasi, K. O., et al., "A compact broadband cross-shaped circularly polarized planar monopole antenna with a ground plane extension," *IEEE Antennas Wireless Propag. Lett.*, Vol. 17, No. 2, 335–338, Feb. 2018.
26. Zhou, C. F. and S. W. Cheung, "A wideband CP crossed slot antenna using  $1-\lambda$  resonant mode with single feeding," *IEEE Trans. Antennas Propag.*, Vol. 65, No. 8, 4268–4273, Aug. 2017.
27. Ullah, U. and S. Koziel, "A broadband circularly polarized wide-slot antenna with a miniaturized footprint," *IEEE Antennas Wireless Propag. Lett.*, Vol. 17, No. 12, 2454–2458, Dec. 2018.
28. Ellis, M. S., Z. Zhao, J. Wu, X. Ding, Z. Nie, and Q.-H. Liu, "A novel simple and compact microstrip-fed circularly polarized wide slot antenna with wide axial ratio bandwidth for C-band applications," *IEEE Trans. Antennas Propag.*, Vol. 64, No. 4, 1552–1555, Apr. 2016.
29. Nosrati, M. and N. Tavassolian, "Miniaturized circularly polarized square slot antenna with enhanced axial-ratio bandwidth using an antipodal Y-strip," *IEEE Antennas Wireless Propag. Lett.*, Vol. 16, 817–820, Sep. 2016.
30. Ojaroudi, Y., N. Ojaroudi, and N. Ghadimi, "Circularly polarized microstrip slot antenna with a pair of spur-shaped slits for WLAN applications," *Microw. Opt. Technol. Lett.*, Vol. 57, No. 3, 756–759, Mar. 2015.
31. Shen, J., C. Lu, W. Cao, J. Yang, and M. Li, "A novel bidirectional antenna with broadband circularly polarized radiation in X-band," *IEEE Antennas Wireless Propag. Lett.*, Vol. 13, 7–10, Dec. 2013.
32. Jan, J.-Y. and J.-W. Su, "Bandwidth enhancement of a printed wide-slot antenna with a rotated slot," *IEEE Trans. Antennas Propag.*, Vol. 53, No. 6, 2111–2114, Jun. 2005.
33. Sung, Y., "Bandwidth enhancement of a microstrip line-fed printed wide-slot antenna with a parasitic center patch," *IEEE Trans. Antennas Propag.*, Vol. 60, No. 4, 1712–1716, Apr. 2012.
34. Zhang, X. and L. Zhu, "Patch antennas with loading of a pair of shorting pins toward flexible impedance matching and low cross polarization," *IEEE Trans. Antennas Propag.*, Vol. 64, No. 4, 1226–1233, Apr. 2016.
35. Pozar, D. M., *Microwave Engineering*, 4th Edition, Wiley, New York, 2011.